The Report Committee for Marlon Wayne Bright
Certifies that this is the approved version of the following report:

GPS L2 C Signal Survey and the Development of the *Emergent MATLAB L2 C* (*EMAL2*) Receiver

APPROVED BY
SUPERVISING COMMITTEE:

Supervisor:

Todd Humphreys

Bob E. Schutz

GPS L2 C Signal Survey and the Development of the *Emergent MATLAB L2 C* (*EMAL2*) Receiver

by

Marlon Wayne Bright, B.S.

Report

Presented to the Faculty of the Graduate School of

The University of Texas at Austin

in Partial Fulfillment

of the Requirements

for the Degree of

MASTER OF SCIENCE IN ENGINEERING

The University of Texas at Austin

December 2012

This report is dedicated to the love of my life, my wife Shirley, and to my family for their unconditional love and tireless dedication to me.

Acknowledgements

I would like to thank Dr. Kenn Gold and Dr. George Davis for the opportunity to work for Emergent Space Technologies on this project over the course of the last year. A special thanks is due to Dr. Gold for allowing me to use this project as a Report topic and for his guidance and support along the way. I would, also, like to thank Dr. Todd Humphreys for challenging me in all of his courses and, in doing so, making my time at the University of Texas very enriching and rewarding. In addition, I thank Dr. Humphreys and Dr. Bob Schutz for their willingness and availability to advise me on this project. Last but certainly not least, I owe a huge debt of gratitude to Ken Pesyna, Jahshan Bhatti, and Kyle Wesson of the UT Radionavigation Lab for supplying me with test data and *GRID* receiver execution outputs. I could not have completed this without their assistance.

Abstract

GPS L2 C Signal Survey and the Development of the *Emergent MATLAB L2 C* (*EMAL2*) Receiver

Marlon Wayne Bright, M.S.E

The University of Texas at Austin, 2012

Supervisor: Todd Humphreys

The United States Department of Defense has introduced two new GPS civilian signals on its "Link 2" (L2) and "Link 5" (L5) center frequencies. The first of these new civilian signals to reach full operational capability in the GPS constellation will be the L2 C signal. The L2 C signal boasts new signal structure features aimed at better tracking performance in comparison to the legacy L1 C/A signal. Amongst these are two new chip-by-chip interleaved spreading code sequences, Civilian Moderate (CM) and Civilian Long (CL), and a new, higher resolution navigation message, CNAV. The two new C codes are longer than the legacy C/A code and feature a data less pilot signal (CL) for improved tracking performance in weak signal environments. This work investigates L2 C acquisition and tracking considerations and implements algorithms for acquiring and tracking the signal in a software-defined receiver developed in *MATLAB*. The *Emergent MATLAB L2 C* (*EMAL2*) receiver was developed for the purpose of GPS signal simulator testing. This software-defined receiver differs from legacy receivers containing application specific integrated circuits (ASICs) in that all of *EMAL2's* digital signal processing is done in software able to run on a general purpose processor. This approach offers greater flexibility and ease in configuration over ASICs for tracking a number of

different types of signal structures in the receiver. The *EMAL2* receiver's design and implementation is described here-in. Initial testing of the *EMAL2* receiver was conducted with live-sky signal data captured by antennas and front-ends at the University of Texas Radionavigation Laboratory (UT RNL). The data was processed by the *GRID* receiver (also at the UT RNL) to provide *EMAL2* baseline received signal characteristics.

Table of Contents

List of Figures

1. Introduction

Since the United States Department of Defense's NAVSTAR Global Positioning System (GPS) reached full operational capability in 1994, military users have enjoyed the use of signals on two different center frequencies known as "Link 1" (L1) and "Link 2" (L2). Civilian users have enjoyed the less precise Standard Positioning Service via an open, coarse acquisition (C/A) signal on the L1 center frequency. Recently, as part of the GPS Modernization effort the US DoD has introduced new civilian signals on its L2 (known as L2 C) and "Link 5" (L5) center frequencies [1]. The first of the Block IIR-M satellites (SVs) capable of broadcasting L2 C was launched in 2005 [2]. As of July 2012 there are currently 9 SVs normally broadcasting the L2 C signal [3]. A full constellation of L2 C and L5 broadcasting SVs is expected in 2019 [1].

By far the greatest benefit of tracking both the L1 C/A and L2 C (or L5) signals is the practical elimination of the greatest remaining GPS signal error source—the ionosphere. The ionosphere is an upper layer of the atmosphere subject to ionization by solar radiation and is a major cause of GPS signal attenuation. The ionosphere has different effects on signals of different frequencies [4]. One can eliminate the first and second order error effects on GPS psuedorange and carrier phase measurements through measurements on at least two, separate frequencies. It is known that dual-frequency measurements can eliminate up to 99%(L1/L2 tracking and "high" signal carrier-to-noise ratios) of the effects of the ionosphere compared to the, at best, 50% error elimination provided by the standard Klobuchar model whose coefficients are broadcast in the GPS navigation message [5]. Codeless tracking methods using the military's P(Y) code have been implemented for dual frequency ionospheric error elimination in the past. However, these methods are more complicated than standard code correlation tracking. The new civil signals eliminate the need for such techniques in many cases.

Both L2 C and L5 feature longer spreading code sequences and a data less pilot sequence [6]. These codes allow for extended coherent integration times in receiver signal processing and are more readily suitable for weak signal tracking applications. The purely civilian L5 signal, purposed for safety-of-life applications, will feature the highest transmit power of the three civil signals and lies in an internationally protected aviation frequency band.

Another benefit in tracking the L2 C (or L5) signal is the utilization of the new and improved CNAV navigation data message. The CNAV data message features a more modern message-based format in contrast to the frame-based format of the legacy NAV message. In addition, satellite ephemeris information will be provided in greater resolution in the CNAV format aiding higher precision navigation solutions [7].

This work focuses on the L2 C signal since it will be the first of the new civil signals to reach full operational capability in the GPS constellation. The L2 C signal advertises averages of 2.7 dB greater data recovery and 0.7 dB greater carrier tracking over the L1 C/A signal, though L2 C is transmitted at a power level 2.3 dB weaker than its L1 C/A counterpart [7].

The rest of this introductory Chapter 1 describes the L2 C signal structure, GPS receiver signal processing in general, and the software-defined receiver approach. Chapter 2 presents the development of a software-defined L2 C post-processing receiver developed in *MATLAB* entitled *EMAL2*. Chapter 3 presents results from live-sky signal testing and validation of the *EMAL2* receiver. Chapter 4 discusses software execution performance comparisons between acquisition of the L1 C/A signal and two different approaches to acquiring L2 C. Chapter 5 gives appropriate conclusions drawn from the presented work. Chapter 6 discusses envisioned future work to expand testing and add functionality to the *EMAL2* receiver as well as migrating the demonstrated L2 C receiver algorithms to a real-time software receiver to be implemented on the Universal Software Receiver Peripheral (USRP) platform.

1.1 L2 Civil Signal Structure

The L2 C signal is nominally broadcast in phase quadrature with the restricted L2 Precision (P(Y)) signal on a sinusoidal carrier with a nominal center frequency of 1227.60 MHz and a signal bandwidth of 2.046 MHz. The civil signal lags the military's precision signal by a phase offset of 90°. L2 C is comprised of two distinct psuedorandom noise (PRN) ranging sequences, the Civilian Moderate (CM) and Civilian Long (CL) codes. Each code sequence is transmitted at 511.5 kHz. The two are chip-by-chip time-division multiplexed together (CM leading CL) to form a combined sequence with a chipping rate of 1.023 MHz (same as L1 C/A). The CM code is 10,230 chips in length giving it a nominal period of 20ms. The 50 symbol/s CNAV, forward error corrected (FEC) navigation message is modulated onto the CM sequence. The CL code is 767,250 chips in length resulting in a nominal code period of 1.5s. Thus, in terms of code period, the CM and CL codes are 20 and 1500 times, respectively, longer than C/A code [7].

The CM and CL codes are generated using the same code generator polynomial in a 27-bit Galois (modular) type linear feedback shift register (LFSR) clocked at 511.5 kHz:

$$1 + X^3 + X^4 + X^5 + X^6 + X^9 + X^{11} + X^{13} + X^{16} + X^{19} + X^{21} + X^{24} + X^{27}$$

Generation of different ranging codes for each SV is accomplished by varying the starting sequence of the LFSR as assigned in Table 3-II of [7]. The CM code generation is short-cycled (reset) every 10,230 chips to achieve CM's 20ms code period. The CL code generation is short-cycled every 767,250 chips to achieve CL's 1.5s code period. A timing diagram of the L2 C code and CNAV symbol train is shown in Figure 1.

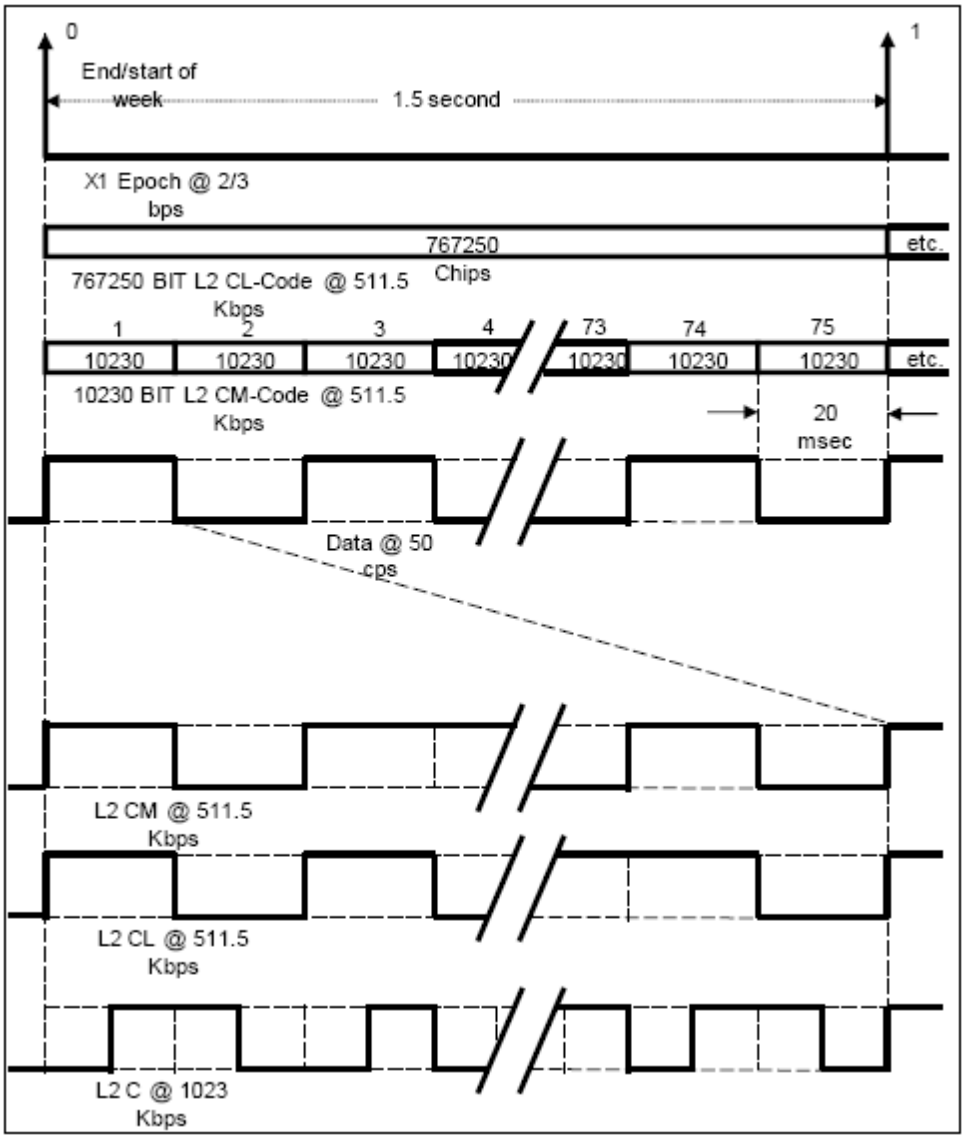

Figure 1: L2 C signal timing diagram. Shows timing relation between CM and CL chips as well as CNAV data symbols [7].

1.2 CNAV Data Message

The CNAV data message is a new data message format broken down into 300-bit long, arbitrarily ordered data messages, differing from the defined order frame format of the legacy NAV message. The CNAV data bits are modulo-2 added to the L2 CM ranging code at a rate of 25 bits per second. The message bit train is rate ½ encoded for

forward error correction purposes resulting in a transmission rate of 50 symbols per second. The convolutional coding is constraint length 7, with encoder logic shown in Figure 2 [7].

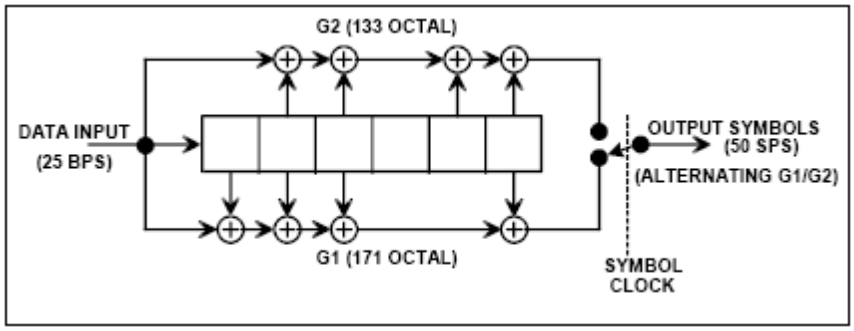

Figure 2: CNAV data message FEC encoder logic [7].

Each 300-bit (12 second) message starts with an 8-bit preamble (binary: 10001011), followed by a 6-bit PRN number of the transmitting SV, a 6-bit message type ID with range of 0 (000000) to 63 (111111), and the 17-bit message time of week (TOW) count. This TOW count multiplied by 6 represents SV time in seconds at the start of the next 12-second message [7].

The broadcast sequence of messages is stated in [7] as completely arbitrary, but sequenced to provide optimum user performance. Most importantly, ephemeris data are broadcast at least once every 48 seconds (1 out of 4 messages). The reader should refer to Appendix III of [7] for the full specification of the CNAV message types and structures.

An additional important note and improvement is that the CNAV data stream is higher precision and nominally contains more accurate data than the standard NAV data. Therefore, data from the CNAV and NAV messages should not be mixed in any algorithms or applications.

1.3 Software-Defined Approach

The classic GNSS (Global Navigation Satellite Systems) receiver contains what are known as application specific integrated circuits (ASICs). These ASICs contain hardware components specifically designed for the correlation of a particular signal structure. Once a design is ready and mass production begins, there are, practically, no inexpensive changes that can be made (i.e. if desiring to take advantage of another signal structure type) [8].

On the contrary, the software-defined GNSS receiver does not contain ASICs and offers a good deal of flexibility in signal tracking. It accomplishes all digital signal processing on a programmable microprocessor rather than a hard-wired discrete component [8]. This provides for post-deployment programmability to reconfigure production characteristics, thus making it generally more cost-effective to develop and update. Figure 3 illustrates a typical software-defined GNSS receiver block diagram.

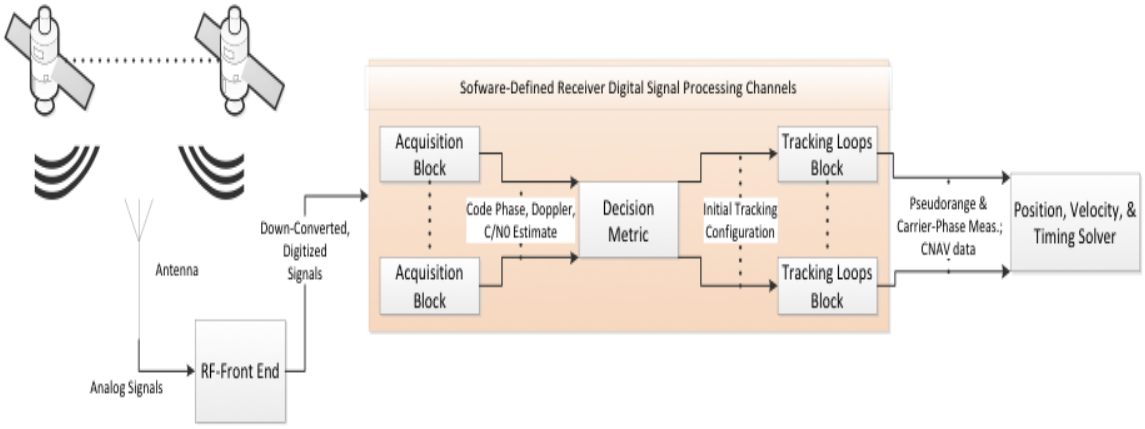

Figure 3: General software-receiver schematic.

It shows that SV broadcast analog signals and background noise are received via the receiver's antenna, filtered, and fed to the RF front-end where the signals are down-converted and sampled. The now digitized front-end data are processed by the acquisition blocks of the (typically) multiple channels of the software defined receiver code. Here, through numerous software-implemented correlations with a locally generated code

replica, a two-dimensional search is conducted for a particular SV's received signal code phase and Doppler frequency offset from the nominal carrier intermediate frequency. A carrier-to-noise estimate of the desired signal is, also, produced.

Next, a decision is made based on these estimates as to whether or not the searched for PRN's signal is present. If a signal is deemed present, the acquired estimates are handed over to tracking loop blocks to refine and maintain these metrics. The loops produce psuedorange and carrier phase measurements to each SV tracked as well as demodulate the transmitted navigation data bits (or symbols). These observables are fed into a position, velocity, and timing solver to produce the receiver's navigation solution.

2. A *MATLAB* Software-Defined GPS L2 C Receiver: *EMAL2*

The *Emergent MAtlab L2 C* (*EMAL2*) receiver developed in this study was based on an open-source GPS L1 C/A receiver developed in [5]. Paired with its L1 C/A counterpart, *EMAL2* is purposed to be an efficient GPS signal simulator testing tool for the *MrSig* project [9] being developed by Emergent Space Technologies. These two tools are ideal for initial signal simulator testing where there is no real-time requirement. Raw signal data generated by the simulator can be recorded and post-processed. All aspects of the received signals' structure, their acquisition, and their tracking can be readily accessed and analyzed with *MATLAB* tools. The pursued approach was to leverage as much of the existing and tested code structure as possible to minimize the complexity of the software development problem and focus in on the changes that tracking the new L2 C signal structure presents.

EMAL2 is initially designed as a single-frequency receiver for stationary terrestrial applications. It does not make use of any handover from L1 C/A. However, in practice, most L2 tracking receivers will possess dual frequency tracking capabilities. Therefore, making use of L1 C/A tracking information to narrow the L2 C search space and thus reduce L2 C signal acquisition time would be wise if available. However, acquiring the L2 C signal first could be advantageous in weak signal environments due to the data less CL code sequence [10].

Figure 4 outlines the post-processing receiver workflow for the *EMAL2* receiver.

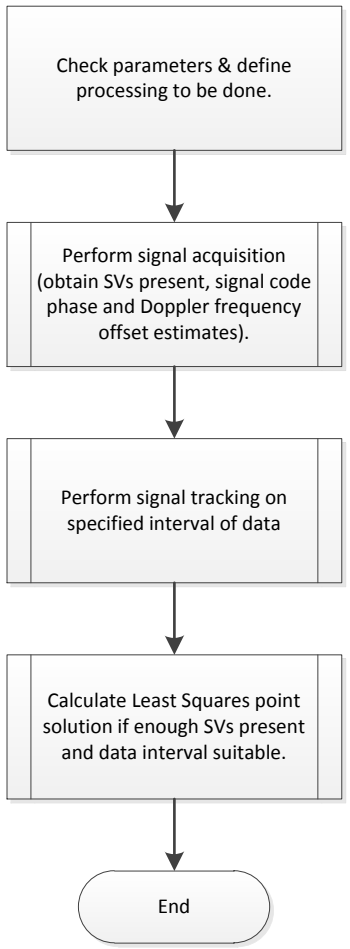

Figure 4: *EMAL2* post-processing receiver workflow.

The *EMAL2* receiver follows the general software receiver diagram though the individual channel processing is done in an asynchronous fashion within each receiver block. We, also, note that at this time, the Calculate Least Squares solution data block was not implemented. The primary reasoning for this is that in the data sets acquired for development, no more than two L2 C broadcasting SVs are present at any given instance in time. Therefore, the required number of SVs for an L2 C-based position and timing solution (four) were not met.

All of the general receiver and raw signal data settings are kept in one central data structure shared by all blocks of the receiver. This is an important software design feature carried over from [5] and is illustrated in the top block of Figure 4.

2.1 Signal Acquisition Block

Acquiring the L2 C signal has the same objective as that of its L1 C/A counterpart. Estimates are sought for a prescribed PRN's code phase, carrier Doppler frequency offset, and signal carrier-to-noise ratio. The process, itself, is a two-dimensional search over all possibilities of PRN code phase and carrier frequency.

The serial search approach to acquisition begins with forming the desired coherent integration length of a local signal replica sampled to the rate of the incoming raw signal data. This replica features the PRN spreading code for the sought after SV and the Doppler offset carrier frequency for the current search space grid point. In practice, for short coherent integration times, like the ones used in this development, any code Doppler frequency offset can be neglected with minimal degradation to the correlation peak power. Next, the local signal replica is shifted with respect to the incoming raw signal data to reflect the code phase being tested in the current trial. Multiplying the raw signal data by the local signal replica, accumulating over the defined integration time, and squaring the result forms the targeted grid point's statistic. Once all values in the two dimensional search grid have been tested, the peak in the resulting statistics is selected as the best estimate for the acquisition objectives.

The PRN codes of L2 C were specially selected for their auto and cross-correlation properties which, essentially, yield a distinct peak only when the local signal replica is aligned in code chip phase and actual carrier frequency. The carrier-to-noise ratio, C/N_0, of a GPS signal is defined in [1] as

(2-1)

$$\frac{C}{N_0} = \frac{A^2}{4\sigma_n^2 T_s}$$

where A is the average signal power, σ_n^2 is the receiver noise variance, and T_s is the sub-accumulation interval used in the acquisition (and tracking) coherent integrations. Carrier-to-noise ratio can be computed from the relation between the search grid's peak value statistic and surrounding noise statistics.

The high-level procedure of the implemented L2 acquisition algorithm is to first acquire the shorter of the two C codes, yielding a CM code phase and coarse Doppler frequency offset estimate. For *EMAL2*, the more efficient Fast Fourier Transform-based (FFT) correlation techniques described in [11] are used for the CM code acquisition in lieu of a serial search approach. The FFT-based correlation techniques take advantage of the principles of the Discrete Fourier Transform to simultaneously search all possible code offsets at a particular frequency.

Now having acquired the CM code phase, the CL code phase search space is narrowed to a total of 75 possibilities. All 75 CL code phase possibilities are tested via serial search methods at the coarse carrier frequency estimate. The peak amongst the results is accepted as the CL code phase estimate. Finally, with the full C code phase estimates now determined, the PRN codes are wiped off of the signal and FFT techniques outlined in Chapter 6 of [5] are used to perform a parallel frequency search for the fine resolution carrier frequency.

The work flow diagram of the signal acquisition block is shown in Figure 5.

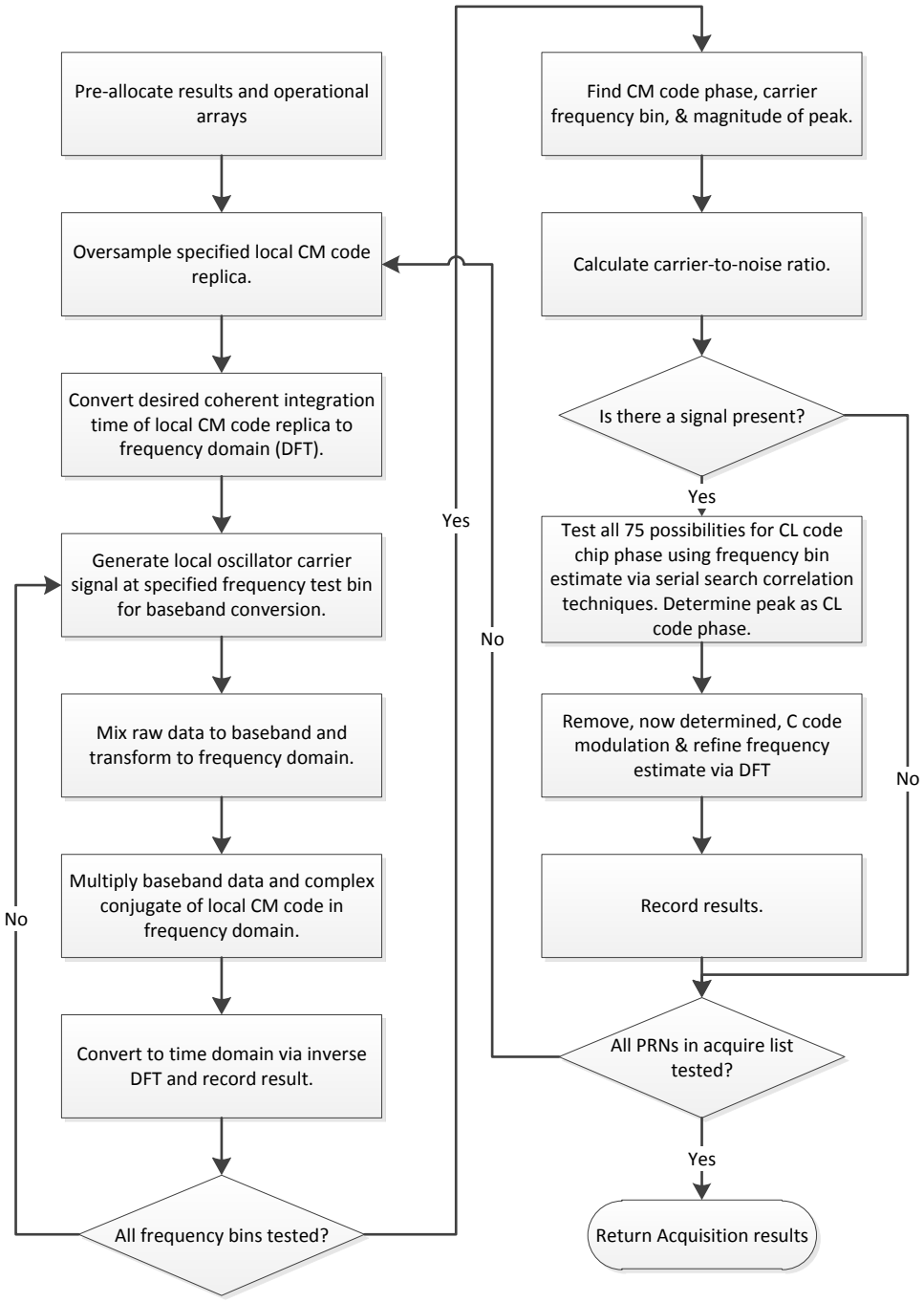

Figure 5: *EMAL2* receiver acquisition function work flow.

As prescribed in [10] and [12], the CL chips of the local replica are zeroed out for the initial CM code acquisition. Thus, the unknown CL code phase does not hurt the signal power obtained in the accumulations, but it does not help either. As a result, it requires twice as long integration intervals in L2 CM or CL only acquisitions to recover the same peak correlation power as a similar L1 C/A correlation. Nominally, the *EMAL2* receiver uses a coherent integration time of 15ms in its initial CM acquisition.

The longer PRN code periods of the L2 CM signal increase the code phase search space in relation to L1 C/A. However, the Doppler frequency search window is smaller by comparison with L1 C/A. This is easily seen in analyzing the expression for Doppler frequency offset, f_D, for electromagnetic waves given in [13]:

(2-2)

$$f_D = -\frac{v_{s,r}}{c} f_0$$

where $v_{s,r}$ is the line-of-sight velocity of the SV relative to the receiver, f_0 is the transmitted frequency, and c is the speed of light through a vacuum. The $v_{s,r}$ term is constant when considering signals from the same SV, though transmitted on different frequencies. Thus, the lower transmitted carrier frequency of the L2 C signal yields a smaller Doppler frequency search window. A computational comparison of direct L2 C acquisition versus L1 C/A acquisition is included in Chapter 4. As stated before, in practice most L2 C tracking receivers will first acquire and track L1 C/A and thus can significantly minimize the acquisition search space for L2 C.

2.2 Signal Tracking Block

Post-acquisition, the acquired PRN code phase and carrier frequency estimates are handed over to the signal tracking block for refinement and maintenance. The primary objectives of the signal tracking block are to provide psuedorange (indirectly) and carrier phase measurements as well as demodulated navigation data bits (symbols). These observables are obtained via implementation of code and carrier tracking loops.

Much research into GPS tracking loop design, implementation, and characteristics has been conducted and is more thoroughly presented in [1] and [5]. More performance and prediction analysis is given in [14] and [15]. The carrier phase tracking loop is, typically, referred to as the Costas Loop or PLL. The code tracking loop is referred to as the Delay Lock Loop or DLL. Both loops can be modeled as second-order phase lock loops comprised of a loop discriminator, first-order filter, and numerically controlled oscillator (NCO). A frequency lock loop (FLL) can, also, be used for carrier tracking and is particularly useful when tracking with the PLL is not possible.

A linearized digital model for a second-order phase lock loop is shown in Figure 6.

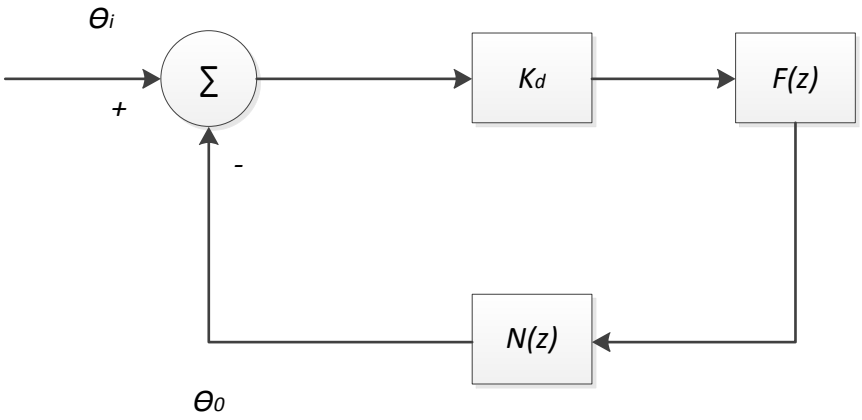

Figure 6: Linearized second-order PLL model.

The transfer functions for the loop filter and NCO are

(2-3)

$$F(z) = \frac{(C_1 + C_2) - C_1 z^{-1}}{1 - z^{-1}}$$

(2-4)

$$N(z) = \frac{K_O z^{-1}}{1 - z^{-1}}$$

respectively. Expressions for the coefficients C1 and C2 were determined as (full derivation in [16])

(2-5)

$$C_1 = \frac{\frac{1}{K_O K_d}(8\zeta\omega_n T)}{4 + 4\zeta\omega_n T + (\omega_n T)^2}$$

(2-6)

$$C_2 = \frac{\frac{1}{K_O K_d}(4\omega_n T)^2}{4 + 4\zeta\omega_n T + (\omega_n T)^2}$$

where $K_O K_d$ is the loop gain, ζ is the damping ratio, T is the sampling time, and ω_n is the natural frequency found as

(2-7)

$$\omega_n = \frac{8\zeta B_L}{4\zeta^2 + 1}$$

where B_L is the noise bandwidth in the loop. Combined, the damping ratio and loop bandwidth control the filter overshoot and settling time. In general, setting these values involves a trade-off between pull-in range and the amount of noise let in the filter. For this implementation, the nominal value for loop noise bandwidth, B_L, is 2 Hz for the DLL and 25 Hz for the PLL to ensure a wide loop pull in range. Smaller bandwidths are desirable for most practical applications. The damping ratio is set at 0.7 for both loops.
The overall loop transfer function is then

(2-8)

$$H(z) = \frac{\theta_0(z)}{\theta_i(z)} = \frac{K_d F(z) N(z)}{1 + K_d F(z) N(z)}$$

2.2.1 Carrier Tracking

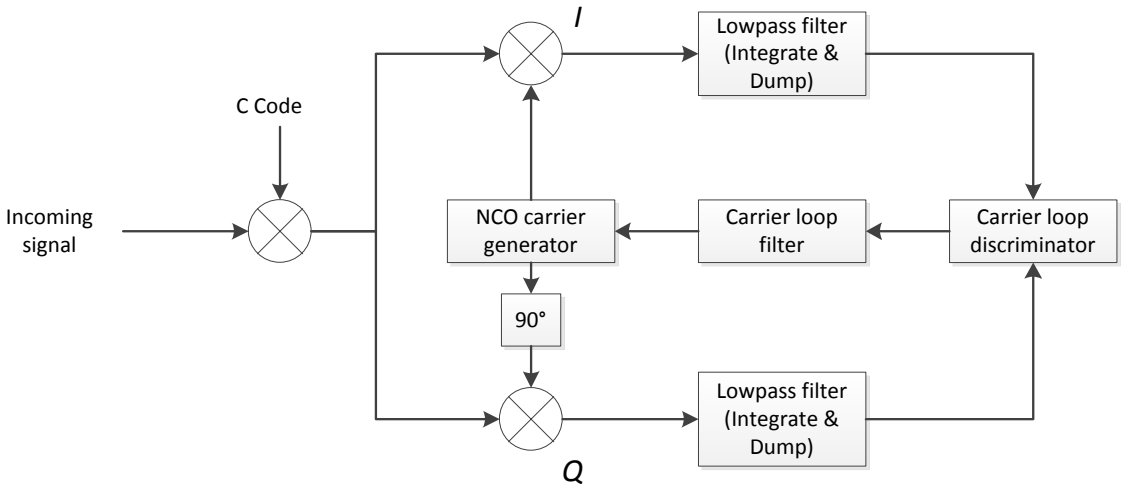

Figure 7: Costas loop diagram.

The *EMAL2* receiver is initially implemented to track the CM code in order to demodulate navigation data symbols. For this purpose we must be insensitive to the 180° phase transitions caused by the data bit modulation. Thus, a Costas loop (shown in Figure 7) is implemented instead of an ordinary PLL [15]. A future extension of this work would be to track CL where an ordinary PLL could be used, avoiding the squaring loss of the Costas Loop.

After code chip wipe off, two multiplications are made. One multiplication is made between the input signal and the local carrier wave. Another is made between the input signal and a 90° phase-shifted version of the local carrier wave. These multiplications distinguish the in-phase (I) and quadrature (Q) arms of the loop. The goal

of the Costas loop is to keep all energy in the in-phase arm. After the low pass filters on each arm the remaining I and Q signals are

(2-9)

$$I = \frac{1}{2} D(n)\cos(\varphi)$$

(2-10)

$$Q = \frac{1}{2} D(n)\sin(\varphi)$$

respectively, where φ is the carrier phase error between the incoming signal and the local signal replica and $D(n)$ is the current navigation data symbol. Note that equations 2-9 and 2-10 are noise free illustrations of the signal and not an actual good signal model. Then the phase error is found as

(2-11)

$$\frac{Q}{I} = \frac{\frac{1}{2} D(n)\sin(\varphi)}{\frac{1}{2} D(n)\cos(\varphi)} = \tan(\varphi)$$

(2-12)

$$\varphi = \tan^{-1}\left(\frac{Q}{I}\right)$$

The arctan discriminator presented in Equation 2-12 is the implemented carrier loop discriminator. It is the most accurate of Costas loop discriminators, though it is the most computationally expensive. Nonetheless, it suits our purpose for post-processing fine. Other loop discriminators can be found in [1].

2.2.2 Code Tracking

The goal of the DLL, also known as an early-late tracking loop, is to control the local replica code generator so that its replica is aligned in time with the received code. As such, its output is a perfectly aligned replica of the code. A partial basic code tracking block diagram is shown in Figure 8.

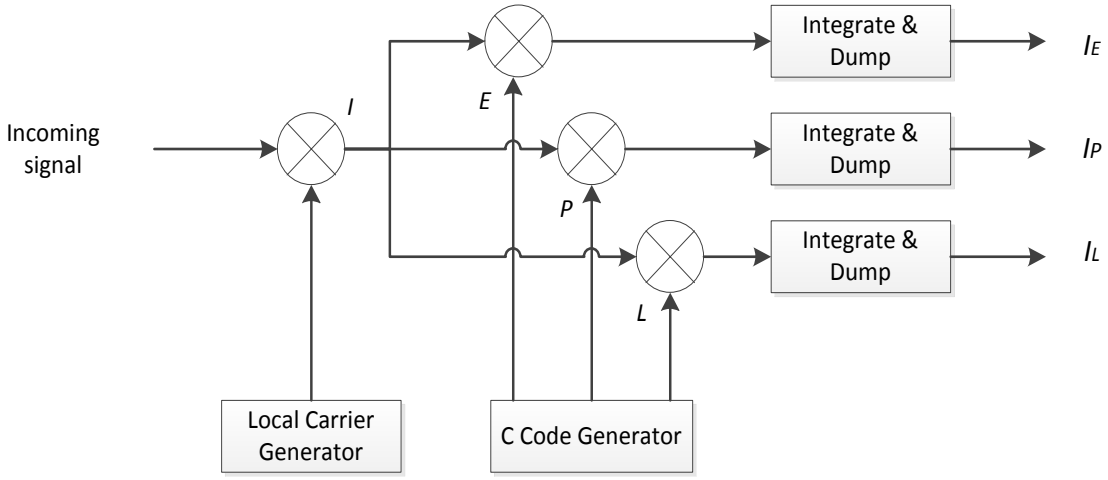

Figure 8: Basic code tracking loop diagram.

The incoming signal is first mixed to baseband by the local carrier wave controlled by the carrier tracking loop. The resulting baseband signal is then correlated with early, prompt, and late versions of the local PRN replica. The replicas in the implemented receiver are nominally generated with a $\pm\frac{1}{2}$ chip offset between them. Depending on the signal tracking scenario, this can be adjusted. A loop discriminator determines which accumulation (Early, Prompt, or Late) provided the most energy and, subsequently, signals the code generator to speed up, slow down, or stay constant in time to keep the two signals promptly aligned. Since the carrier tracking loop may not always be exactly locked, a similar quadrature arm is added to make the performance of the code tracking loop independent of that of the carrier tracking loop.

The implemented loop discriminator is the noncoherent normalized early-minus late power discriminator

(2-13)

$$D = \frac{(I_E^2 + Q_E^2) - (I_L^2 + Q_L^2)}{(I_E^2 + Q_E^2) + (I_L^2 + Q_L^2)}$$

The normalization allows this discriminator to be used with signals of different strengths. Other discriminators exist and are presented in [1] and [5].

2.2.3 Combined Code and Carrier Tracking and Software Implementation

The carrier and code tracking loops can be combined as one block to reduce the required number of computations for signal tracking. One such set up for this is shown in Figure 9.

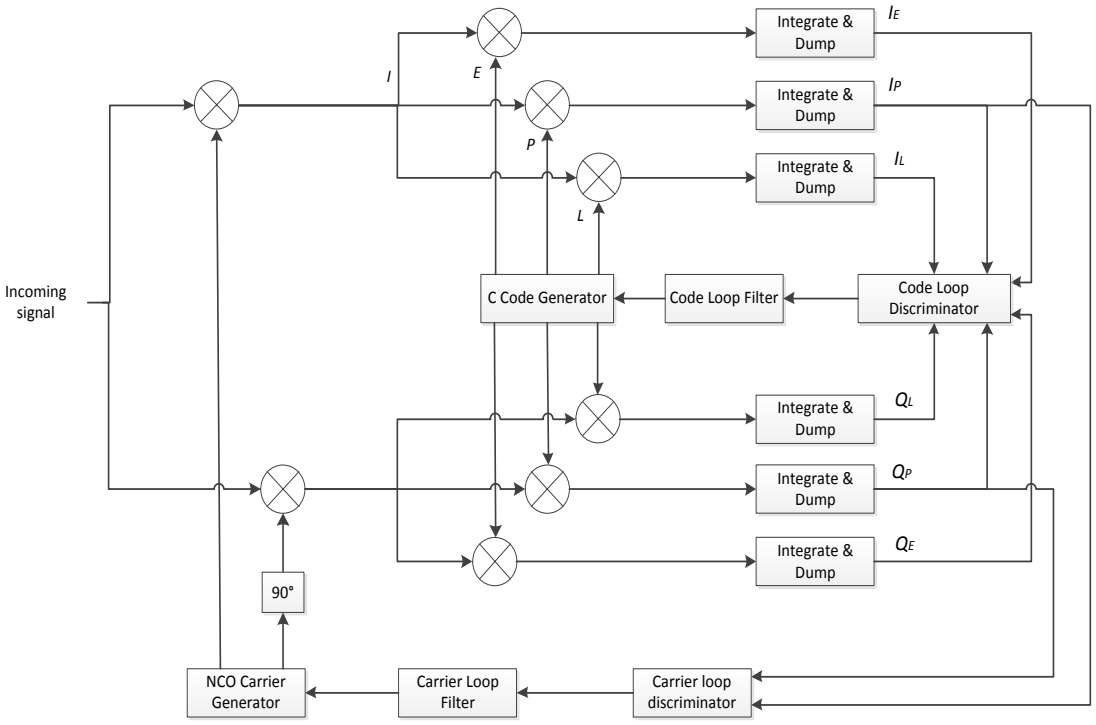

Figure 9: Combined carrier and code tracking loops.

The block diagram of the *EMAL2* combined carrier and code tracking function is shown in Figure 10. Nominally, the *EMAL2* receiver implements 8 channels for signal tracking.

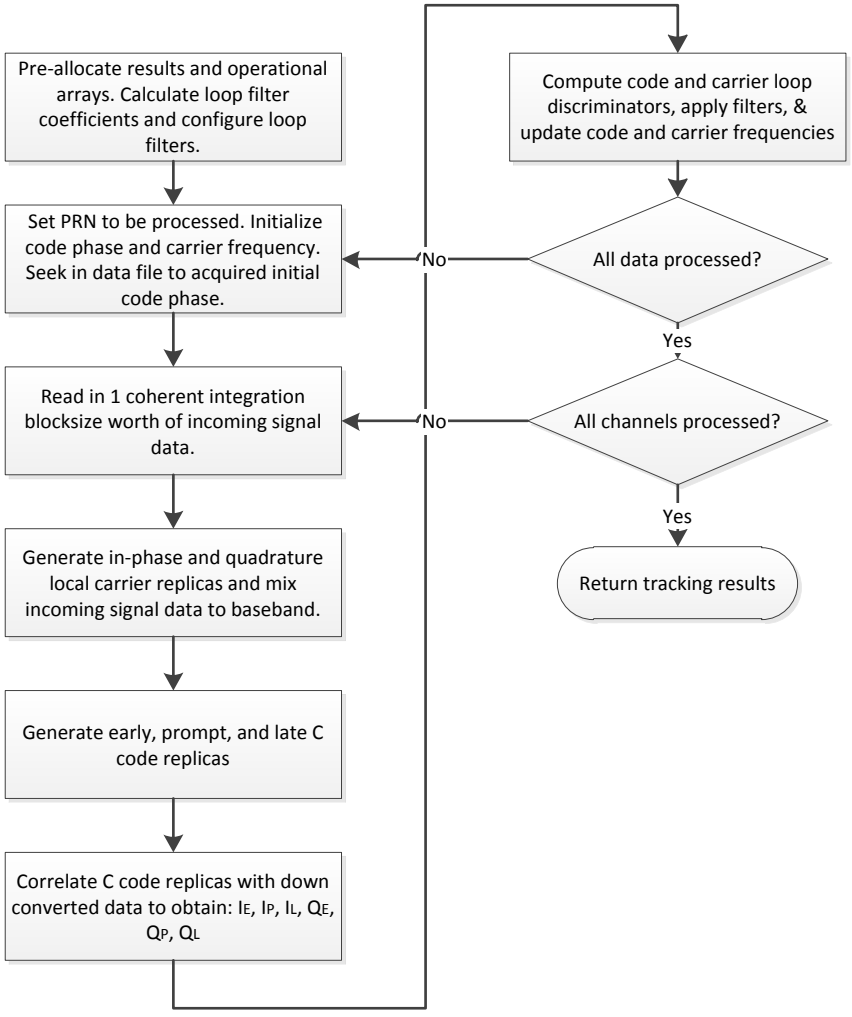

Figure 10: *EMAL2* tracking function block diagram.

3. Initial Receiver Testing

Initial testing of the *EMAL2* receiver was conducted with live-sky signal data taken from two different RF front-ends at the University of Texas Radionavigation Laboratory (UT RNL). The first of the employed front-ends was a Mitel GP2015 model. For L2 frequency data samples, the GP2015 outputs 2-bit (sign and magnitude) quantized real data at intermediate frequency 1.399 MHz and at a sampling rate of 5.714 MHz [17]. The other of the employed front-ends was a Bobyn GPS L1/L2 front-end model that produces 2-bit quantized real L2 C data at an intermediate frequency of 1.610 MHz and a sampling frequency of 5.714 MHz [18]. These front-ends both use received analog signals from a GPS antenna on the roof of W. R. Woolrich Laboratories on the University of Texas campus.

Three different data sets were recorded on different days for a total of four signal tracking scenarios. Data set 1 was recorded on July 28, 2008 (GPS Week 1490) from the Mitel GP2015 front-end featuring one strong (PRN 31) and one moderate strength signal (PRN 29). Data set 2 was recorded on May 7, 2010 (GPS Week 1582) from the Bobyn L1/L2 front-end and contains one weak L2 C signal (PRN 7). Data set 3 was recorded on August 3, 2012 from the Bobyn L1/L2 Front-End and features one strong L2 C signal (PRN 7). The raw sample files were processed by the multi-frequency, science grade, *GRID* receiver [19] and its output was used as truth data. In each of the signal tracking instances, the *EMAL2* receiver's performance over time intervals ranging from ~175 to ~600s was compared to that of the *GRID* receiver in two metrics: signal Doppler frequency estimate and carrier-to-noise ratio. These metrics were chosen because they are important signal tracking results and are readily accessible in each receiver. On the contrary, things like raw code phase estimates are difficult to solicit from production receivers like *GRID* whose tracking internals are not typically accessible.

After verifying that the *EMAL2* receiver acquired the same moderate ($> 38dB - Hz$) to high carrier-to-noise ratio L2 C signals as the *GRID* receiver (full acquisition

results are given in the Appendix) tracking comparison plots are given in Figures 11 through 14.

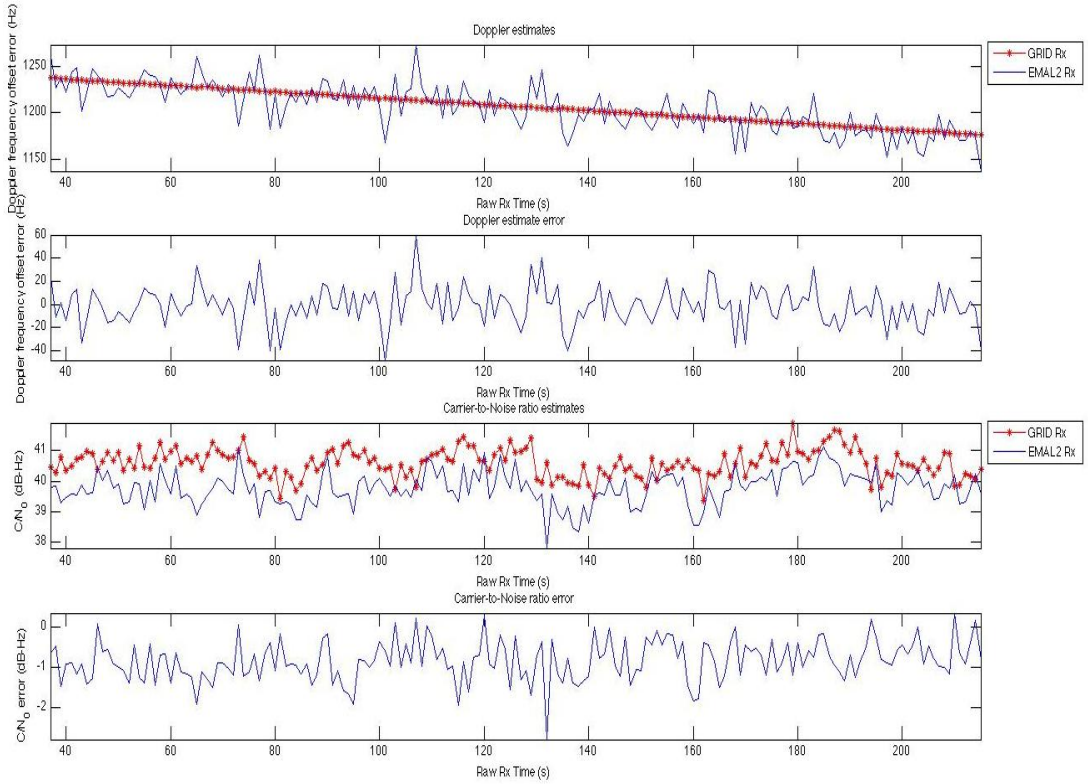

Figure 11: PRN 29 tracking comparisons (*EMAL2* vs. *GRID*), July 28, 2008

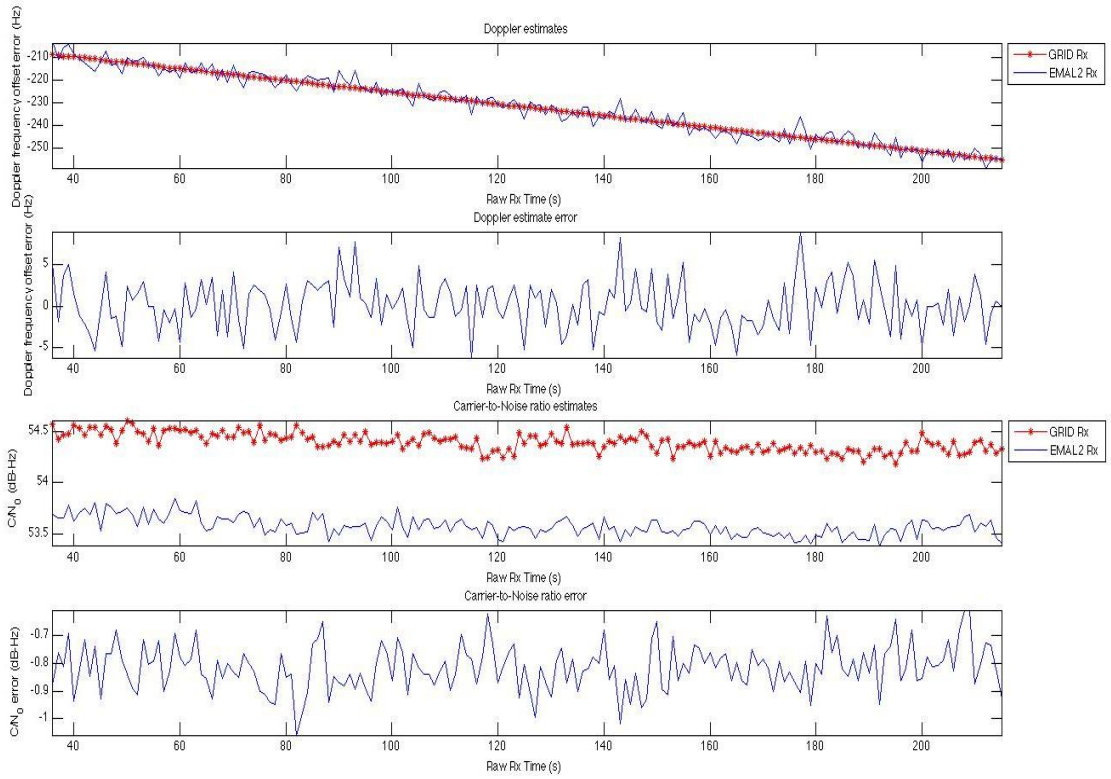

Figure 12: PRN 31 tracking comparisons (*EMAL2* vs. *GRID*), July 28, 2008

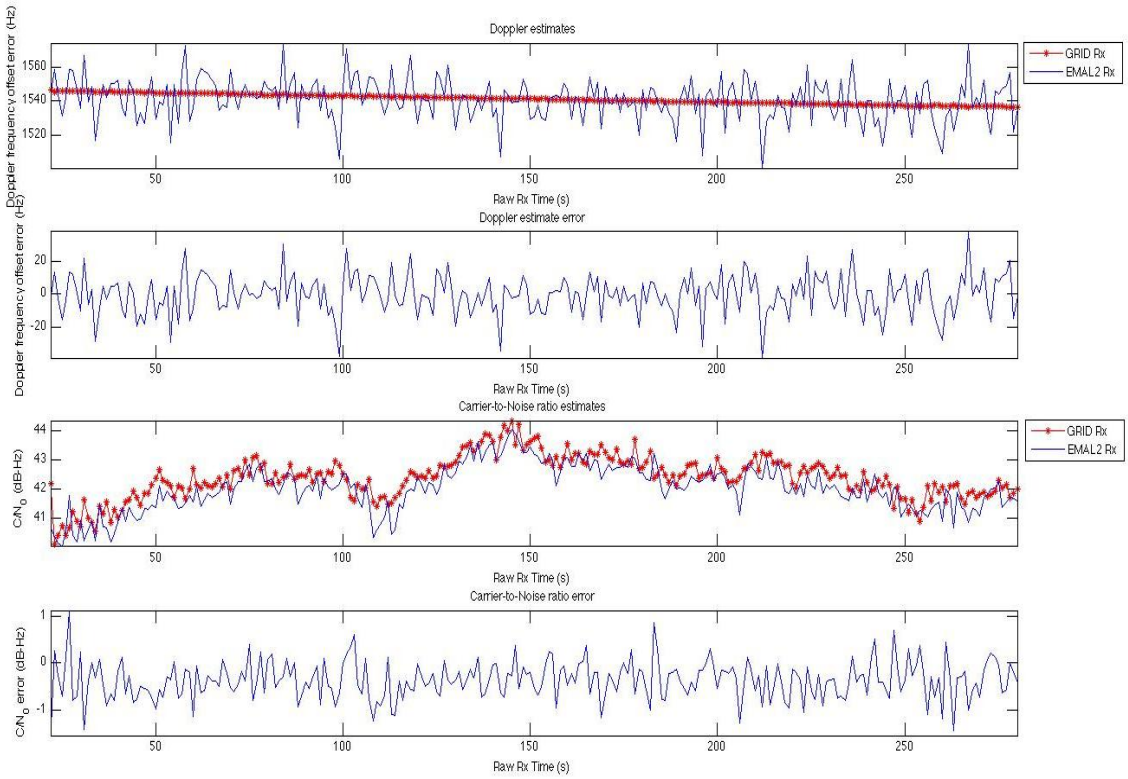

Figure 13: PRN 7 tracking comparisons (*EMAL2* vs. *GRID*), May 7, 2010

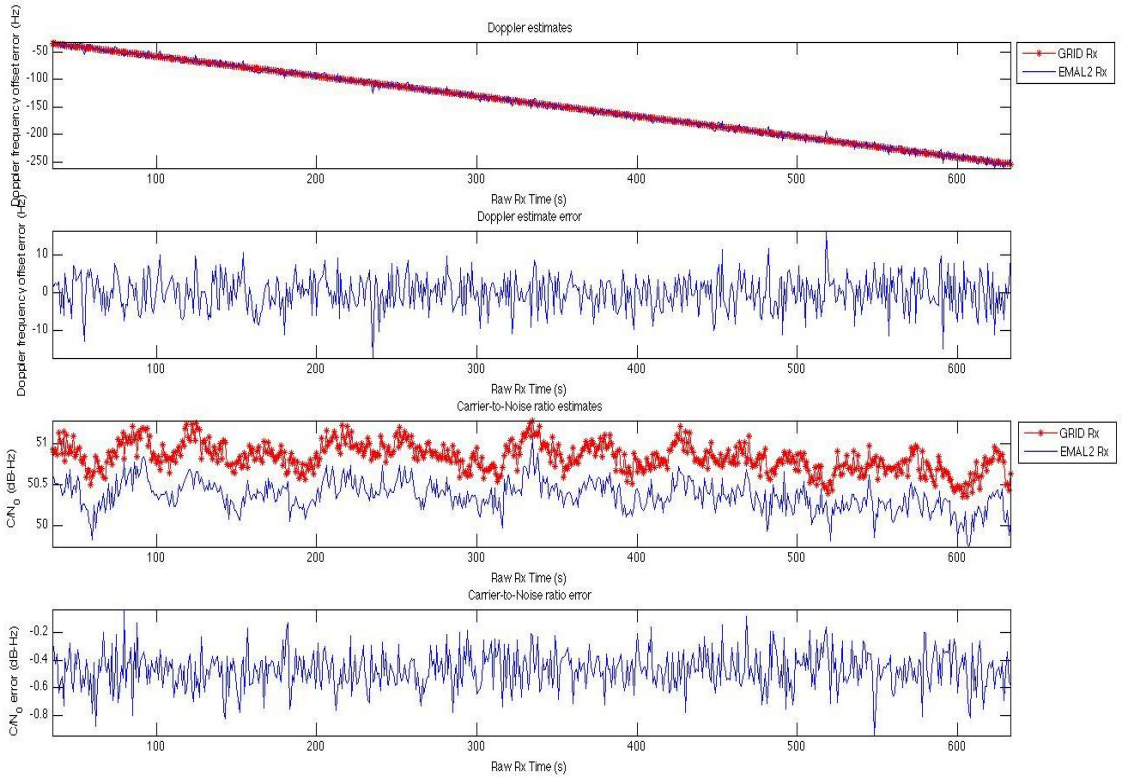

Figure 14: PRN 7 tracking comparisons (EMAL2 vs. GRID), August 3, 2012

Figures 11-14 plot *EMAL2*'s estimates of signal Doppler frequency offset and carrier-to-noise ratio as well those of the *GRID* receiver and the former's error as calculated against the latter. Both receivers' plots have the same general trends. The errors between the two are bounded for both comparison metrics. A statistical analysis of the tracking comparison, summarizing the results in Figures 11 through 14, is given in Table 3-1.

Table 3-1: Initial Testing Tracking Comparison Summary

Date	PRN	Length of Comparison Interval (s)	Avg. C/N_0 *GRID* (dB-Hz)	Avg. C/N_0 *EMAL2* (dB-Hz)	*EMAL2* C/N_0 RMS Error (dB-Hz)	*EMAL2* RMS Doppler Error (Hz)
7/28/08	29	178.000034	40.593	39.760	0.976	16.576
7/28/08	31	179.007034	54.391	53.576	0.819	2.970
5/7/10	7	258.015697	42.374	42.009	0.546	11.917
8/3/12	7	598.001125	50.834	50.366	0.487	4.612

EMAL2 matches *GRID*'s estimates better on the stronger signals in the set. This can be expected as *EMAL2* only has one tracking configuration at this point and thus does not make adjustments for optimal weak signal operation. From Appendix 12A and p. 494 of [1], it is given that we can expect the performance of *EMAL2*'s carrier tracking loop to be within the frequency error variance

$$var\{\Delta f\} = \frac{B_{f,1}N}{2\pi^2(N-1)^2T_{CO}^2\left(\frac{C}{N_0}\right)}\left(1+\frac{N-1}{2\left(\frac{C}{N_0}\right)T_{CO}}\right)$$

where $B_{f,1}$ is the one-sided noise bandwidth of the loop filter, N is the number of coherent integration intervals participating in the non-coherent integration, and T_{CO} is the coherent integration time. For the first signal tracking instance of PRN 29 on 7/28/08, the expected frequency error variance is

$$var\{\Delta f\} = \frac{25Hz(2)}{2\pi^2(2-1)^2(.001)^2(9642.67)}\left(1+\frac{2-1}{2(9642.67).001}\right) = 281\ Hz^2$$

where the specified one-sided loop filter bandwidth was $25Hz$, the number of non-coherent integrations, N, was set to its minimum of 2, a $.001s$ coherent integration time was used, and the calculated carrier-to-noise ratio was converted to the appropriate linear units by $\left(\frac{C}{N_0}\right)_{linear} = 10^{\frac{\left(\frac{C}{N_0}\right)_{logarithmic}}{10}}$. Similarly, the expected variances can be calculated as $11.1\ Hz^2$, $165\ Hz^2$, and $23.4\ Hz^2$ for the final three tracking instances. Thus, we would expect RMS tracking errors of $16.8Hz$, $3.33\ Hz$, $12.8Hz$, and $4.84Hz$, respectively, for each signal tracking instance. *EMAL2's* errors are in the same ballpark, thus its carrier-tracking performance is deemed suitable. We note here that *EMAL2's* error was calculated in relation to the *GRID* receiver which, as good as it may be, has its own theoretical error which is not readily calculated with the typically provided information. The numbers in Table 3-1 do not exactly coincide due to differences in the implemented acquisition and tracking algorithms of the two receivers.

For the carrier-to-noise ratio estimates, the *GRID* receiver employs a bitwise correlation technique that is not employed in the *EMAL2* receiver [19]. The local replica signal is not two-bit quantized in the same fashion as the incoming samples and correlations between the two signals are performed as 64-bit value multiplications. The ratio itself in the *EMAL2* receiver is not calculated via an expression derived from the probabilistic statistics of the incoming data samples as in the *GRID*. It is calculated via the less precise, but valid approach of averaging accumulation peak values and comparing them to accumulation value averages where no signal is present.

EMAL2's Doppler estimate errors appear as noise on the *GRID* produced estimates. This can most probably be attributed to differences in the tracking loop bandwidth and damping ratio tuning parameters between the receivers. *EMAL2*'s parameters are tuned in such a way to allow greater dynamic range for the loop, but as a consequence more

noise is allowed through the loop filter. This is a necessary consequence for *EMAL2* to robustly pull-in a wide range of acquisition Doppler estimate errors without implementing an FLL or specific, pull-in phase PLL.

EMAL2's acquisition products as well as full signal tracking outputs for data set 1 are given in the Appendix.

4. Acquisition Execution Performance Comparisons to Legacy L1 C/A Receiver

We find it helpful to attempt to quantify the cost of directly acquiring the L2 C signal versus acquiring and tracking L1 C/A only or acquiring L1 C/A as a means to narrow the search space for L2 C acquisition. However, the optimal approach is primarily dictated by the signal environment (i.e. weak signals, high multi-path, etc.). Tracking execution performance for L2 C can be made much the same as the L1 C/A signal (changing the local replica C/A code for C code), and, thus, is not discussed in detail here. However, the L2 CL signal is data free and therefore can be tracked without the computationally expensive arctan discriminator.

In order to compare the execution performance of L1 C/A acquisition to direct L2 CM Acquisition, we make the following assumptions for the sake of comparison:

- The PRN chipping rates for both data streams are the same [7].
- The sampling frequency, f_s, is the same for both data streams.
- The coherent integration time is 1ms for both data streams to make signal correlation and integration computations at a single point on the 2-D grid search space in the serial search acquisition approach the same number of processor computations for both L1 C/A and L2 C signals (of course the size of the search spaces are different).
- The L1 C/A terrestrial Doppler offset search range is $\pm\, 7kHz$ and we will use a coarse bin spacing of $250Hz$ for a total of

(4-1)

$$2 \times \left(\frac{7000}{250}\right) + 1 \;=\; 57 \text{ frequency bins}$$

to test. From the calculation (derived from Equation 2-2 for signals from one SV) that

(4-2)

$$f_{D_{L2}} = \left(\frac{f_{L2}}{f_{L1}}\right) \times f_{D_{L1}} = \left(\frac{1227.60}{1545.42}\right) \times 7000Hz \approx 5500Hz$$

the L2 Doppler search range for stationary terrestrial applications can safely be reduced to $\pm$ 5.5 kHz. Keeping a bin spacing of 250 Hz, this yields

(4-3)

$$2 \times \left(\frac{5500}{250}\right) + 1 \; = \; 45 \text{ frequency bins}$$

to test.

- The practical overhead of mixing to baseband the longer minimum required size incoming signal data stream of L2 C (40ms for CM and 1500ms for CL) versus that of L1 C/A (2ms) is negligible.
- Once the coarse acquisition search is complete, the same number of computations are required to perform the fine resolution frequency search for both the L1 C/A and L2 C signals.

4.1 Serial Search Acquisition Method

For our serial search acquisition method, we have shown that for the above provided assumptions the number of processor computations for a signal correlation and integration at a single search grid point is the same for both the L1 C/A and L2 CM signals. Therefore, their difference in total number of computations is based solely on the number of search grid points to test. For L1 C/A, we have

(4-4)

$$.001s \times f_s \text{ code phase possibilities} \times \; 57 \text{ frq bins} \; = \; .057 \times f_s \text{ grid points}$$

For L2 CM, we have

(4-5)

$$.020s \times f_s \text{ code phase possibilities} \times \ 45 \text{ frq bins } = \ .900 \times f_s \text{ grid points}$$

and for L2 CL

(4-6)

$$1.5s \times f_s \text{ code phase possibilities} \times \ 45 \text{ frq bins } = \ 67.5 \times f_s \text{ grid points}$$

Assuming that each grid point calculation takes constant time and are executed in sequential fashion, direct L2 CM acquisition is

(4-7)

$$\frac{.900 \times f_s \text{ grid points}}{.057 \times f_s \text{ grid points}} = \ 15.789 \text{ times}$$

more costly than L1 C/A acquisition. Similarly, direct L2 CL acquisition is

(4-8)

$$\frac{67.5 \times f_s \text{ grid points}}{.057 \times f_s \text{ grid points}} = \ 1184.2 \text{ times}$$

more costly than L1 C/A acquisition.

Many dual frequency receivers do not attempt direct acquisition of the L2 C signal. They first acquire the L1 C/A signal and use the C/A code phase and Doppler frequency offset estimate to narrow the search range for the L2 C signal. The Doppler frequency offset estimate of the L1 signal can be mapped to L2 by Equation 4-2 and is thus specified. Since CM and CL code start times are synchronized with C/A start times, there are 20 and 1500 possibilities for CM and CL code phase respectively. Thus, the CM acquisition starts out with $57 \times f_s$ grid points worth of 1ms correlations and coherent

integrations. To that we add an additional 20 grid points to test for the CM code phase for a

(4-9)

$$\left(1 - \frac{.057 \times f_s + 20}{.900 * f_s}\right) * 100\%$$

improvement over direct CM acquisition. For an example sample frequency of f_s = 5.714 MHz, the serial search execution time is improved by 93.67%. Once CM is acquired, another 75 possibilities are tested to determine the CL code phase. That is a

(4-10)

$$\left(1 - \frac{.057 \times f_s + 20 + 75}{67.5 * f_s}\right) * 100\%$$

improvement of direct CL acquisition. For our example f_s of 5.714 MHz, the improvement is 99.91%.

4.2 FFT-Based Parallel Code Phase Acquisition Search

For a parallel code phase acquisition search implemented with Fourier Transform techniques, the execution improvement numbers are not quite as drastic. However, a full analysis of FFT-Based parallel code phase search algorithms is dependent on the implementation of the Fast Fourier Transform on the target system and thus is fairly complex and will not be given much effort here. The main idea is that we can reduce our number of implemented search loops from 2 down to 1 (only over the possible Doppler frequency bins). Besides the 12 frequency bin difference between L1 C/A and L2 C, the main distinction between the two acquisition algorithms is the size of the FFT used. At minimum, L1 C/A will need $n_{FFTpts_{L1CA}} = 2ms \times f_s$, with the $1ms \times f_s$ length local replica code zero-padded out to the length of the incoming data stream. L2 CM will need a minimum $n_{FFTpts_{L2CM}} = 40ms \times f_s$, with the local replica code samples zero padded

out to meet the length of the incoming data buffer (may as well extend the coherent integration interval as well). In addition, for most implementations of the FFT it is either required or, at minimum, optimal for n_{FFTpts} be of radix 2 length.

Also of note in the FFT algorithm is that the most common algorithm discussed in [5] (and the one implemented) requires both an FFT and an inverse FFT (IFFT). Like the serial search algorithm, above, many dual-frequency receivers use acquisition results from L1 C/A to narrow the search range for L2 C. Thus, one could acquire L1 C/A with the performance improvements of FFT techniques and then use a serial search approach to test the 20 remaining possibilities for CM and then 75 more for CL, if desired.

5. Conclusions

The L2 Civilian signal brings with it a new signal structure, navigation message type, and the benefits of dual frequency receiver tracking. The new signal structure is appealing in that it offers a data less pilot signal for increased signal tracking performance. The new CNAV data structure offers higher resolution and nominally higher precision navigation data for more precise position and timing solutions. An L2 C tracking post-processing receiver in MATLAB known as *EMAL2* has been developed based on a related L1 C/A receiver. *EMAL2* was tested with live-sky signal data and its estimates compared to those of the *GRID* receiver to verify suitable operation. *EMAL2* was found to have an average RMS error in Doppler frequency offset estimates of 9.019 Hz and an average carrier-to-noise ratio estimate RMS error of 0.707 $dB-Hz$ in comparison to the *GRID* receiver. From a serial search acquisition approach, direct L2 CM acquisition is over 15 times more expensive than L1 C/A. However, serial search execution time for CM acquisition is improved 93.67% when results from L1 C/A acquisition are used in a handover operation.

6. Future Work

Immediate future work involves extending the *EMAL2* receiver's capability to process space-based scenario signal data. This will entail widening the Doppler frequency search window and necessary adjustments to the receiver tracking loop parameters [20]. In addition, weak signal acquisition and tracking techniques involving the CL sequence will be explored and implemented to improve testing functionality for high orbit scenarios. Once a space-based tracking mode is implemented, a navigation solution block to process CNAV navigation data modulated on the CM PRN sequence will be implemented and tested with a full L2 C broadcasting constellation data generated with Spirent simulator data.

Finally, a real-time dual frequency GPS L1 C/A and L2 C receiver for use with the GNU Radio Project's USRP will be developed in *C++* based on existing L1 C/A receiver code. It is planned that this receiver will make use of an acquisition handover algorithm from L1 C/A, to L2 CM, to L2 CL to maximize acquisition execution performance efficiency.

Appendix – Full *EMAL2* Operational Outputs

The following sections contain plots generated by the *EMAL2* receiver in its acquisition and tracking operations for data set 1 described in Chapter 3. Note that some are generated solely in debug operation of the receiver.

Acquisition

As stated in Chapter 2.1 acquisition in *EMAL2* is first performed using the shorter CM code resulting in a CM code phase and coarse carrier frequency estimate. These estimates are formed by correlating the incoming signal with a local signal replica generated by code and carrier frequency estimates across the entire 2-D grid of possibilities. That 2-D grid of accumulated and squared results when the sought after signal is present is shown in Figure 15.

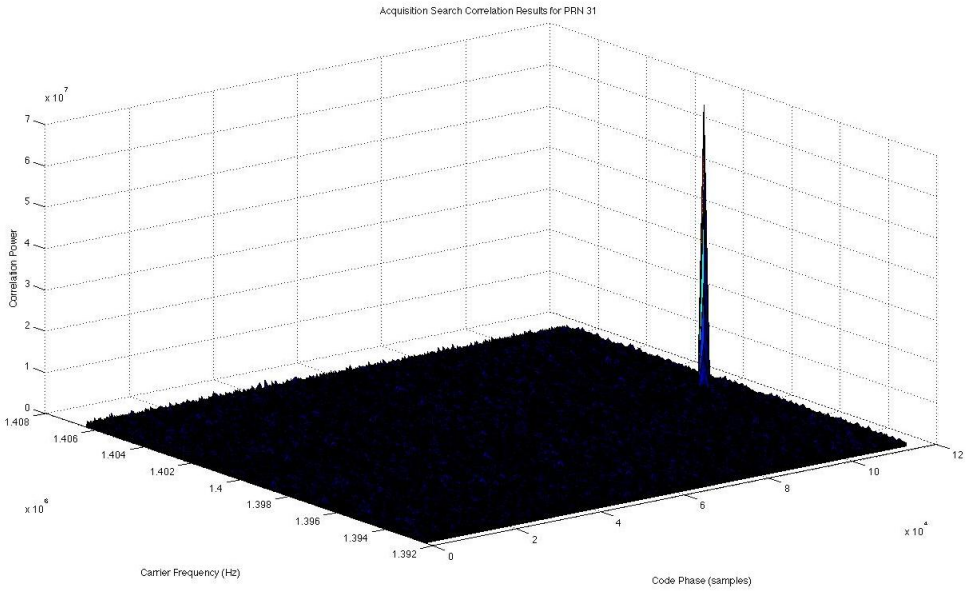

Figure 15: Acquisition search correlation results, PRN 31. July 28, 2008

When the sought after signal is not present no such peak is visible. That scenario is illustrated in Figure 16.

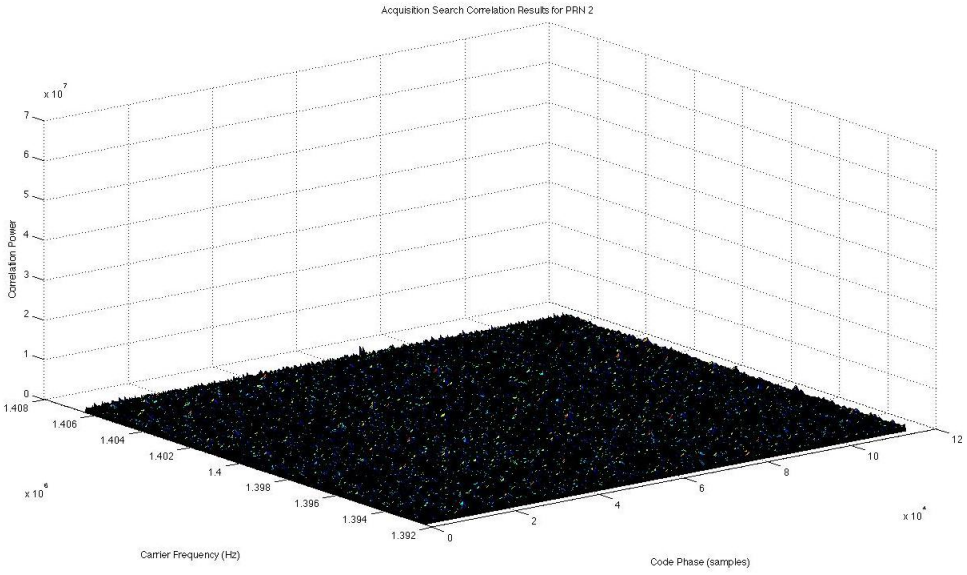

Figure 16: Acquisition search correlation results, PRN 2. July 28, 2008

If a signal is deemed present as shown in Figure 15, the next step is to determine CL code phase in order to be able to wipe off the C code modulation from the incoming signal. Once the start sample of a CM code is known, there are only 75 possibilities remaining for CL code phase. All of these possibilities are tested, shifting the CL replica by one CM code period length between each trial, at the coarse carrier frequency determined in the initial CM acquisition. Results from such a test are shown in Figure 17.

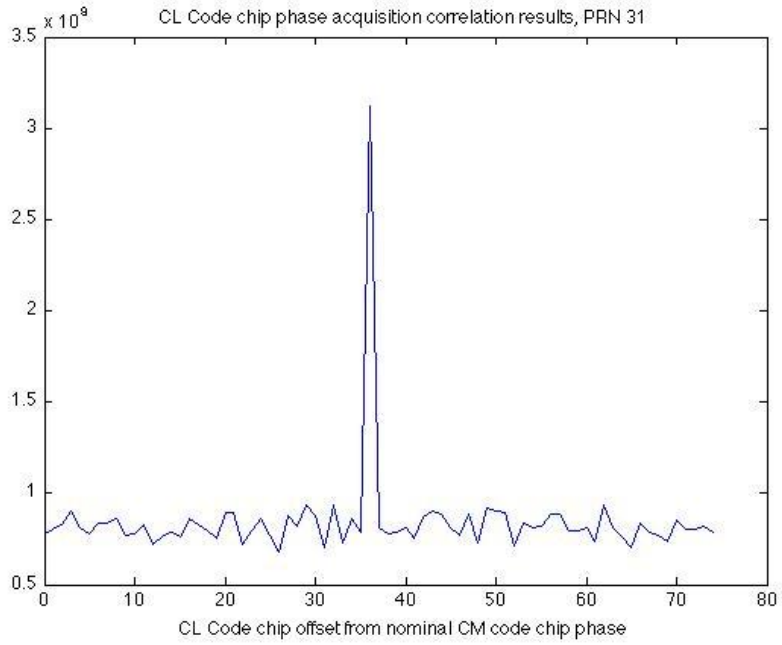

Figure 17: CL code chip phase acquisition correlation results, PRN 31. July 28, 2008

The number of interest here is the CL code shift value (*x*-axis) corresponding to the peak. This number multiplied by the length of the CM code period represents the starting chip of a CL code. In this case, it's 37.

After the full C code phase is determined, the spreading codes are wiped off of the incoming signal leaving only a data modulated carrier. A fine frequency resolution search is performed using FFT-based parallel frequency search techniques on an interval of the incoming carrier that does not straddle a data bit transition. Results from this technique are shown in Figure 18 where the peak corresponds to the fine resolution carrier frequency.

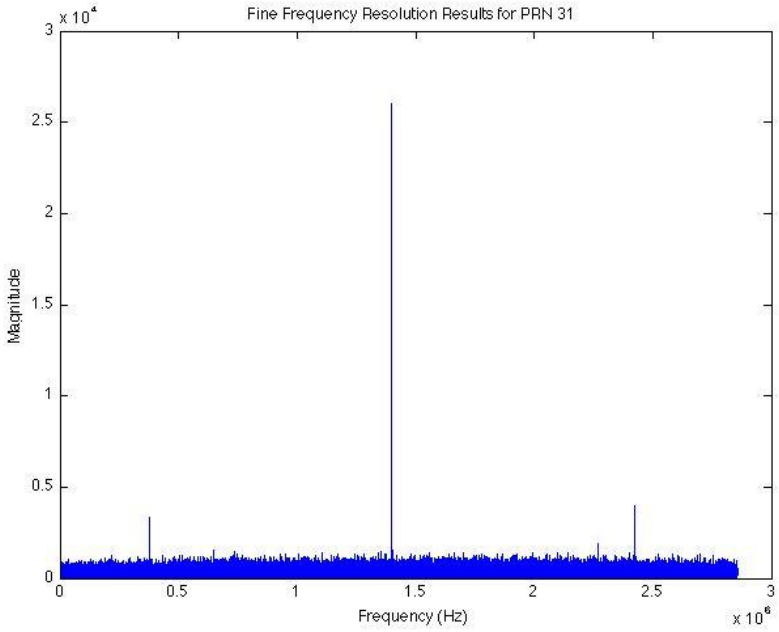

Figure 18: Fine frequency resolution results, PRN 31. July 28, 2008

This process is repeated for all SVs listed in the acquisition search list. However, if CM code based acquisition fails, there is no need to continue (except in weak signal scenarios). An acquisition results summary in terms of acquired carrier-to-noise ratio for data set 1 is given in Figure 19.

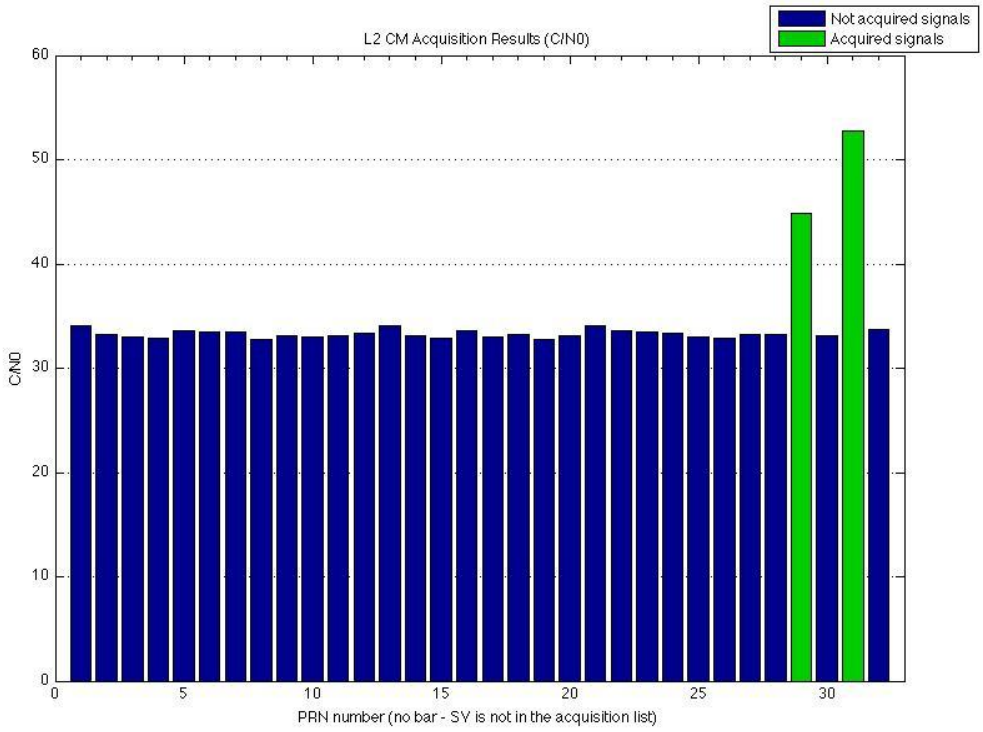

Figure 19: L2 CM Acquisition results, July 28, 2008

The acquired carrier-to-noise ratios for all signals searched for are illustrated. Signals having carrier-to-noise ratio above $38\,db-Hz$ were accepted as present and handed over to the tracking block. In this case, PRNs 29 and 31 are accepted for tracking.

Tracking

From Chapter 3.1, PRNs 29 and 31 were deemed present in data set 1. This is as verified with *GRID* receiver produced data. The *EMAL2* produced tracking results over a 180s time span for both PRNs' signals are shown in Figures 20 and 21.

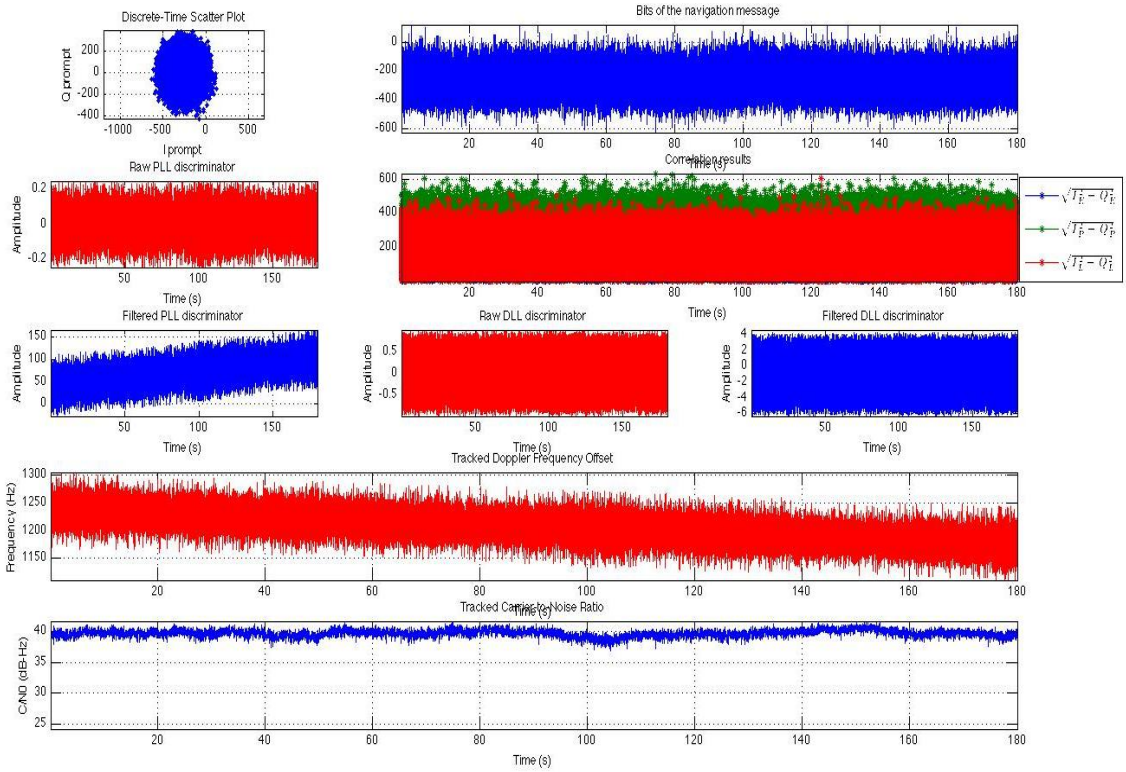

Figure 20: PRN 29 tracking results, July 28, 2008

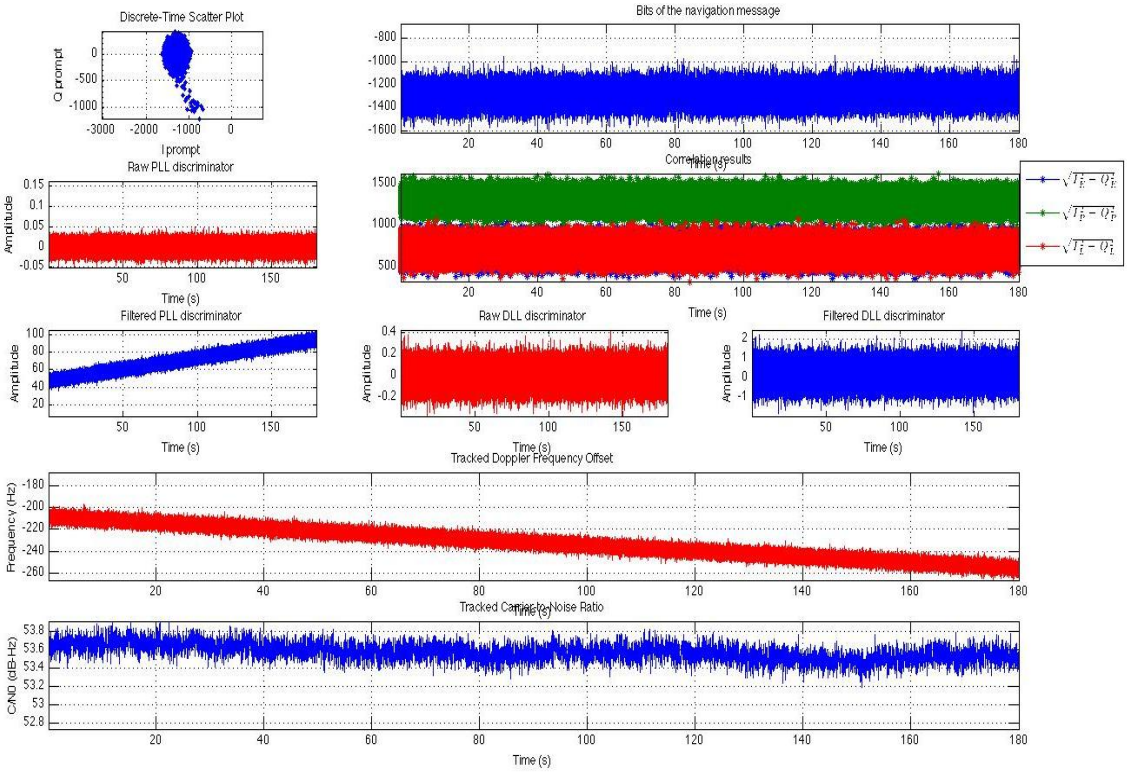

Figure 21: PRN 31 tracking results, July 28, 2008

Figures 20 and 21 give the full tracking loop outputs including the raw and filtered DLL and PLL outputs; early, prompt, and late correlator outputs; signal Doppler frequency offset and carrier-to-noise ratio; and the demodulated navigation bits. Comparisons to GRID receiver produced estimates were given in Chapter 3.

References

[1] Misra, Pretap and Per Enge. *Global Positioning System: Signals, Measurements, and Performance*. Revised 2nd ed. Lincoln, MA: Ganga-Jamuna Press, 2011.

[2] "GPS Modernization". *United States Department of Commerce, Office of Space Commercialization*. Website. 19 July 2012.

[3] "GNSS Modernization". *Unavco*. Website. 19 July 2012. <http://facility.unavco.org/general-info/gnss-modernization/gnss-modernization.html>

[4] Klobuchar, John A. "Ionospheric Effects on GPS". *GPS World*, "Innovation" Column. April 1991.

[5] Borre, Kai, et al. *A Software-Defined GPS and Galileo Receiver: A Single-Frequency Approach*. Boston: Birkhauser, 2007.

[6] Smeyers, S. *An Assessment of the GPS L5 Signal Based on Multiple Vendor Receivers*. Master's report, The University of Texas at Austin, December 2011.

[7] NAVSTAR GPS Space Segment/Navigation User Interfaces, IS-GPS-200, Revision E. *Global Positioning System Wing (GPSW) Systems Engineering & Integration*. 8 June 2010.

[8] B. M. Ledvina, M. L. Psiaki, S.P. Powell, and P.M. Kintner, "Real-Time Software Receiver Tracking of GPS L2 Civilian Signals using a Hardware Simulator" in *Proc. of ION GNSS 18th International Technical Meeting of the Satellite Division*, Long Beach, CA, 13-16 September 2005, pp. 1598-1610.

[9] Emergent Space Technologies. *Multi-Purpose Radio Signal Generator*. NASA Phase II SBIR: Goddard Space Flight Center. POP: 6/1/2011-5/31/2013.

[10] Psiaki, M. L. "FFT-Based Acquisition of GPS L2 Civilian CM and CL Signals" in *Proc. Of ION GNSS 17th International Technical Meeting of the Satellite Division* Long Beach, CA, . 21-24 Sept. 2004.

[11] Yang, C., “FFT Acquisition of Periodic, Aperiodic, Puncture, and Overlaid Code Sequences in GPS,” in *Proc. Of the ION GPS 2001*, Sept. 11-14, 2001, Salt Lake City, UT, pp. 137-147.

[12] Chung Yang. “Joint Acquisition of CM and CL Codes for GPS L2 Civil (L2C) Signals” in *Proc. Of ION 61st Annual Meeting/The MITRE Corporation & Draper Laboratory*, Cambridge, MA, 27-29 June 2005, pp. 553-562.

[13] Rosen, Joe; Gothard, Lisa Quinn (2009). *Encyclopedia of Physical Science*. Infobase Publishing. p. 155. ISBN 0-8160-7011-3.

[14] Ziemer, Rodger E. & Peterson, Roger L. *Digital Communications and Spread Spectrum Systems*. New York: MacMillan, 1985.

[15] Best, Roland E. *Phase-Locked Loops: Design, Simulation, and Applications*. 5th edition. New York: McGraw-Hill, 2003.

[16] Chung, B.-Y.; Chien, C.; Samueli, H.; Jain, R.; , "Performance analysis of an all-digital BPSK direct-sequence spread-spectrum IF receiver architecture," *Selected Areas in Communications, IEEE Journal on* , vol.11, no.7, pp.1096-1107, September 1993.

[17] Zarlink Semicondunctor Inc., 2007. *GP2015: GPS Receiver RF Front End*. Datasheet. Available at: <www.zarlink.com/zarlink/gp2015-datasheet-sept2007.pdf>

[18] D. Bobyn. *L1/L2 GPS Receiver Front End Hardware Technical Description*. Technical report, Cornell University, 2010.

[19] Humphreys, T.E., M.L. Psiaki, P.M. Kintner, Jr., B.M. Ledvina, "GNSS Receiver Implementation on a DSP: Status, Challenges, and Prospects," Proceedings of ION GNSS, The Institute of Navigation, Fort Worth, TX, 2006.

[20] Joplin, A. *Development and Testing of a Miniaturized, Dual-Frequency, Software-Defined GPS Receiver for Space Applications*. Master’s thesis, The University of Texas at Austin, December 2011.